ACS Macro Letters
Letter
pubs.acs.org/macroletters

High-Aspect-Ratio Perpendicular Orientation of PS-*b*-PDMS Thin Films under Solvent Annealing

Jeong Gon Son,[†,‡] Kevin W. Gotrik,[†] and C. A. Ross[†,*]

[†]Department of Materials Science and Engineering, Massachusetts Institute of Technology, Cambridge, Massachusetts, 02139, United States

[‡]Photo-Electronic Hybrids Research Center, Korea Institute of Science and Technology, Seoul, 136-791, South Korea

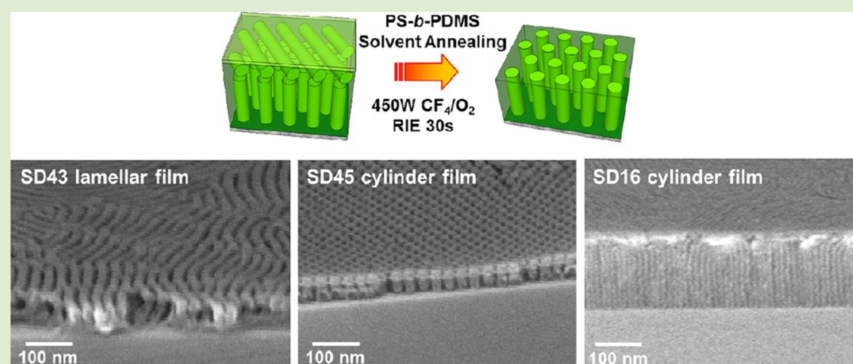

ABSTRACT: A perpendicular orientation of high-aspect-ratio polystyrene-*block*-polydimethylsiloxane (PS-*b*-PDMS) cylindrical and lamellar PDMS microdomains was achieved by solvent annealing and then slowly drying thick PS-*b*-PDMS films. Perpendicularly oriented microdomains occurred throughout the film thickness, except at the air interface, where a layer of in-plane microdomains formed due to the surface energy difference between PS and PDMS. In contrast, thermal annealing produced in-plane orientation throughout the film thickness. The solvent-annealed perpendicular orientation was observed for cylindrical morphology PS-*b*-PDMS of 16 and 45 kg/mol, where PDMS is the minority block, and lamellar PS-*b*-PDMS of 43 kg/mol. To obtain fully perpendicular microdomain patterns, a nonselective high-powered 450 W CF_4/O_2 reactive ion etching process was performed to remove the top layer of the films. Substrate patterning using electron beam lithography produced local registration of 17 nm period hexagonal cylinder patterns.

In microelectronic device manufacturing, a feature half-pitch of approximately 22 nm represents the limit of conventional photolithographic methods with 193 nm immersion photolithography.[1] Alternative approaches for forming sub-22 nm features, such as electron beam lithography and extreme UV lithography, have drawbacks in terms of cost and throughput. In contrast, block copolymer microphase separation spontaneously generates microdomains with period of a few nm and above, and thin films of block copolymers can therefore be used to form nanoscale patterns over a large area in a fast, low cost process. Thus, many research groups have studied block copolymers for potential applications in nanolithography and device fabrication.[2−7]

To use a block copolymer film for sub-20 nm pattern generation, a high Flory−Huggins interaction parameter χ and good etch selectivity between the blocks are required to allow small period features to be formed and for one block to be subsequently removed. In addition, a perpendicular orientation of cylindrical or lamellar microdomains forms high-aspect-ratio patterns which are convenient for certain methods of pattern transfer. Polystyrene-*block*-polymethylmethacrylate (PS-*b*-PMMA) has good etch selectivity,[7] and it can readily form perpendicularly oriented microdomains by controlling the surface chemistry[8] and substrate roughness[9] or by using electric fields[7] or surfactants[10] because the two blocks have similar surface energies. However, $\chi_{\text{PS-PMMA}} \sim 0.06$ at room temperature,[11] which is modest, giving a lower bound to the size of microdomains that can be formed. Other block copolymer systems, such as PS-*block*-polyethylene oxide (PS-*b*-PEO),[12] polystyrene-block-polymethylmethacrylate-block-polyethylene oxide (PS-*b*-PMMA-*b*-PEO) triblock copolymer,[13] and PS-*b*-PEO with organosilicate,[14] have been explored to obtain microdomains with smaller dimensions. Perpendicular orientation of the PS-*b*-PEO/organosilicate microdomains was produced in a solvent annealing process with humidity control or mixed solvents, but this system required subsequent high temperature processing to remove the organic components.

Polystyrene-*block*-polydimethylsiloxane (PS-*b*-PDMS) is attractive for nanolithography on the sub-10 nm length scale because it has a high χ parameter ($\chi_{\text{PS-PDMS}} \sim 0.27$)[15] and high etch selectivity between the blocks.[11] Highly ordered sub-10

Received: September 11, 2012
Accepted: October 10, 2012
Published: October 17, 2012

© 2012 American Chemical Society

nm width lines,[16−18] dots,[19,20] and complex patterns[18,21,22] have been achieved from this block copolymer using trenches[16,17,19] and nanopost templates[18,20] to guide the self-assembly. However, it is a challenge to obtain a perpendicular orientation of cylindrical or lamellar microdomains because of the large difference in surface energy γ between PS ($\gamma_{PS} \sim 40.7$ mN/m) and PDMS ($\gamma_{PDMS} \sim 20.4$ mN/m),[23] which promotes formation of a layer of PDMS at the air interface.

In this letter, we demonstrate high-aspect-ratio perpendicular orientation of cylindrical and lamellar microdomains in PS-*b*-PDMS block copolymer films using solvent annealing combined with reactive ion etching (RIE). We first describe the process for 16 kg/mol PS-*b*-PDMS with a volume fraction of PDMS of $f_{PDMS} = 0.31$, designated SD16, which has a cylindrical morphology in bulk and a period $L_0 = 18$ nm. Films ∼300 nm thick were produced on either brush-coated or as-received silicon wafers from a 5 wt % solution of the block copolymer in cyclohexane. Films were annealed either by thermal annealing at 170 °C for 3 days or by solvent annealing in acetone vapor. The solvent anneal was performed by placing the samples into a glass Petri dish with glass or quartz plate lid[17] in which $V_s = \sim 1$ cm^3 acetone was present. The leak is caused by a small gap between the chamber and its lid. The surface area of the liquid acetone was $S = 4.8$ cm^2 and the total chamber volume was 9.3 cm^3. The S/V ratio (V is the empty volume of the chamber = $(9.3 - V_s)$ cm^3), which we used earlier to parametrize the solvent anneal process,[17] took values of 0.54, 0.56, 0.58, 0.60, and 0.66 cm^{-1} for solvent volumes of $V_s = 0.5$, 0.75, 1.0, 1.25, and 2.0 cm^3, respectively. The acetone fully evaporated within 4 h, after which the samples were removed.

Figure 1 shows the results from SD16 films. The microdomains were imaged by using a 50 W CF_4 RIE for 3 s to remove the thin PDMS wetting layer (∼4 nm) present at the top surface, followed by an O_2 RIE for 20 s to partly etch the exposed PS domains leaving oxidized PDMS visible as bright contrast. Both thermally annealed and solvent annealed films formed in-plane cylinders at the top surface of the films, seen in Figure 1a. However, in the cross-sectional SEM images, while the thermally annealed films showed in-plane hexagonally packed cylinders throughout the thickness (Figure 1b), the solvent annealed films showed perpendicular orientation in the bulk of the film (Figure 1c,d). For the untreated Si wafer, the perpendicular orientation was present at the substrate/film interface (Figure 1c, e, and f), while the films on a PDMS brush-coated Si wafer formed perpendicular orientation only in the middle of the film and parallel orientation at the substrate/film interface (Figure 1d). We showed previously that the surface chemistry of the substrate affects the self-assembly of thin films of PS-*b*-PDMS, with a PDMS brush enhancing the annealing kinetics.[11] However, the PDMS-coated substrate caused a PDMS layer to form at the interface, promoting an in-plane orientation at the substrate.

To obtain high-aspect-ratio cylinders throughout the film thickness, it is necessary to remove the in-plane oriented top layers of microdomains, shown schematically in Figure 2a. This was done with a high power 450 W CF_4/O_2 RIE which removes both PS and PDMS at a similar rate. The acetone-annealed films had in-plane cylinders at the top surface (Figure 2b) but after removing the top 60 nm of the BCP films using 450 W CF_4/O_2 RIE for 15 s followed by a 20 s O_2 RIE to etch into the PS, a perpendicular cylinder orientation was seen over part of the film (Figure 2c). Further etching to a depth of 120 nm revealed a dominant perpendicular orientation (Figure 2d and 2e). Therefore, the in-plane cylinders were present in a top layer that had a thickness between 60 and 120 nm (∼3−6 L_0), and underlying this, the cylinders had a perpendicular orientation.

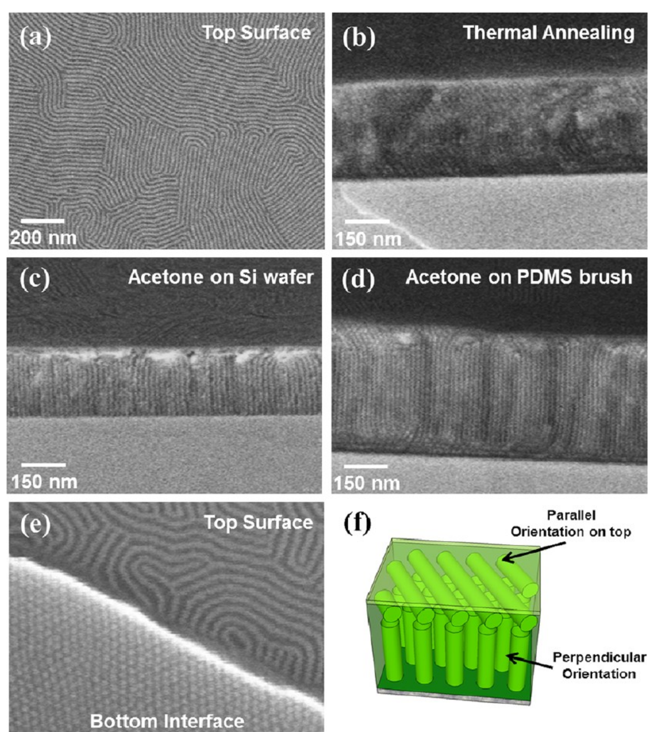

Figure 1. Microdomain orientation of 16 kg/mol PS-*b*-PDMS thick films (>200 nm). (a) Top surface of acetone-annealed BCP film. Cross-section SEM images of films (b) thermally annealed at 170 °C for 2 days, (c) acetone vapor annealed on pristine Si wafer, and (d) acetone annealed on a PDMS brush-coated wafer. (e) Acetone annealed BCP film deposited on a pristine 50 nm SiO_2 coated wafer, as in (c). The film was dissolved from the substrate and folded over when it was immersed in 5 wt % HF aqueous solution. The top-right region shows the morphology of the top surface, while the bottom-left region shows the morphology at the substrate/film interface. (f) A schematic of the solvent annealed PS-*b*-PDMS film in (e).

This perpendicular orientation could also be formed in PS-*b*-PDMS with other molecular weights and morphology. Figure 3 shows perpendicular orientation of lamellae from a 43 kg/mol $f_{PDMS} = 0.50$ PS-*b*-PDMS (SD43) and cylinders from 45 kg/mol $f_{PDMS} = 0.31$ PS-*b*-PDMS (SD45) films using solvent annealing followed by a high power CF_4/O_2 RIE process. The 43 kg/mol film was ∼250 nm thick and was solvent annealed in acetone ($V_s = 1.5$ cm^3 acetone). Figure 3a,b shows high-aspect-ratio line-space patterns with 100 nm height and 42 nm period from SD43. SD45 formed perpendicular cylinders after annealing with chloroform. Figure 3c,d shows 80 nm high, 36 nm period close-packed cylinders with a 29 nm diameter.

The perpendicular orientation was sensitive to the vapor pressure of the solvent and annealing time, which was altered by changing the amount of solvent. In the case of the SD45, $V_s = 0.75$ cm^3 of chloroform was the optimum condition to obtain perpendicular orientation, Figures 3c and 3d. With 1.25 cm^3 of chloroform, there was a larger fraction of in-plane cylinders even after removing the top 120 nm of the film, while a lower vapor pressure (0.5 cm^3 of chloroform, Figure 4b) gave cylinders with greater curvature.

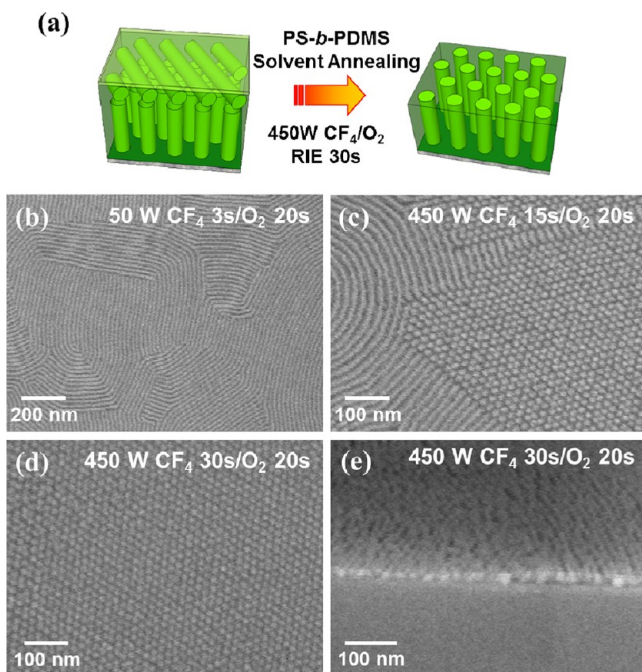

Figure 2. Reactive ion etching (RIE) process for removing top layers of 160 nm thick 16k PS-*b*-PDMS block copolymer film microdomains. (a) A schematic of the structure of PS-*b*-PDMS films on a Si wafer without a brush after solvent annealing then RIE. (b) Top surface morphology treated by 50 W CF_4 RIE for 3 s and then O_2 RIE for 20 s. (c) 60 nm etched morphology treated by 450 W CF_4/O_2 RIE for 15 s and then O_2 RIE for 20 s. (d) In-plane and (e) cross-section SEM images of 120 nm etched morphology treated by 450 W CF_4/O_2 RIE for 30 s and then O_2 RIE for 20 s.

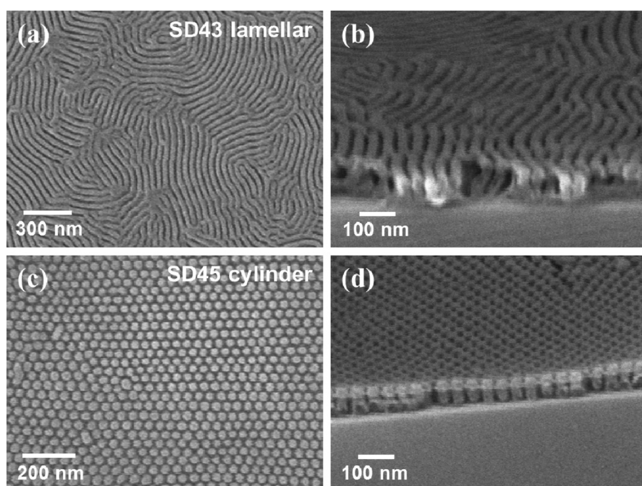

Figure 3. Perpendicular oriented lamellar and cylindrical PS-*b*-PDMS block copolymer thin films after 450 W CF_4/O_2 RIE etching and 90 W O_2 RIE. (a) In-plane and (b) cross-section FE-SEM images of perpendicular lamellar morphology from 43k PS-*b*-PDMS thin film under acetone vapor annealing. (c, d) Perpendicular cylinder morphology from 45k PS-*b*-PDMS thin film under chloroform vapor annealing. The horizontal feature in the film in (d) is believed to be caused by partial removal of the PS from the top surface before sectioning and etching from the side.

To understand the effects of the solvent on the microdomain morphology, it is necessary to determine the time evolution of the solvent vapor for different initial amounts of solvent. First, the weight loss of the annealing chamber was measured as the solvent evaporated for the case of 0.75 cm^3 chloroform (Figure 5a), 2 cm^3 chloroform, and 2 cm^3 acetone (not shown). From the density of the solvents, this indicated a flow rate of 5.16 mm^3/min for chloroform and 5.52 mm^3/min for acetone. The rate of weight loss was the same for the different initial amounts of chloroform, which showed that the leak rate was independent of the amount of solvent in the chamber, at least in the initial stages of the experiment while liquid solvent remained. The solvent was fully evaporated after ~380 min for 2 cm^3 acetone or chloroform and ~150 min for 0.75 cm^3 chloroform.

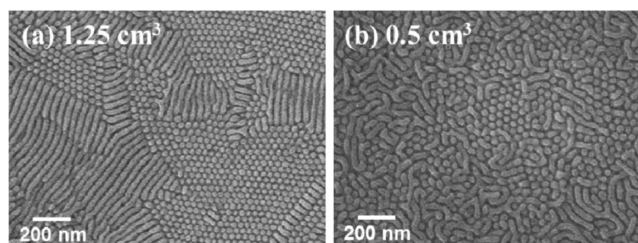

Figure 4. Solvent vapor pressure effects on the orientation of 45 kg/mol cylindrical PS-*b*-PDMS block copolymer. Films ~300 nm thick were treated with 30 s of 450 W CF_4/O_2 RIE and then 30 s of 90 W O_2 RIE. Annealed with (a) 1.25 cm^3 and (b) 0.5 cm^3 of chloroform.

In separate experiments the swelling ratio of SD45 films was measured versus time for different solvent volumes. (To enable the in situ swelling ratio measurements, the glass lid of the chamber was replaced with a quartz plate, but this had only a small effect on the leak rate, decreasing it by a few percent.) Figure 5a,b shows the swelling ratio versus time for SD45 in chloroform. In each case the film swelled quickly to a swelling ratio of ~2.1 and then deswelled over a period of up to 1 h. The maximum swelling ratio increased slightly with solvent volume, from 2.1 to 2.2. This is less than the swelling ratio of SD45 in a closed container of chloroform, which is 2.3−2.4, showing that the beaker with the leak exposed the sample to a solvent vapor pressure slightly smaller than the saturated vapor pressure (i.e., 198 Torr for chloroform at room temperature, 25 °C). Figure 5c shows that the maximum swelling ratio was independent of film thickness in the range of 30−300 nm.

To quantify the swelling behavior, we define time T_1 as the time taken for the swelling ratio to drop to 1.55, that is, half way between 1 and the maximum swelling ratio of approximately 2.1. T_1 = 130 min for 0.75 cm^3 chloroform, Figure 5a. By comparing the rate of loss of the solvent with the swelling ratio, T_1 corresponded to the time at which only about 0.07 cm^3 of chloroform remained in the chamber. About 160 min was required for all the liquid chloroform to evaporate from the weight change. (The amount of saturated chloroform vapor present within the chamber corresponds to only 0.008 cm^3 liquid.)

Figure 5b shows swelling ratios for four different amounts of solvent. T_1 increased almost linearly with the initial solvent amount, Figure 5c inset. These data indicate that the films swelled to their maximum value and remained at that value for a time approximately proportional to the initial amount of solvent. As the liquid solvent became exhausted, the vapor pressure dropped and the film dried and deswelled over about an hour, independent of the initial solvent amount.

In comparison to the slowly dried films described above, rapidly quenched films showed a different microdomain orientation. Rapid quenching of films by exposing the sample

dx.doi.org/10.1021/mz300475g | ACS Macro Lett. 2012, 1, 1279−1284

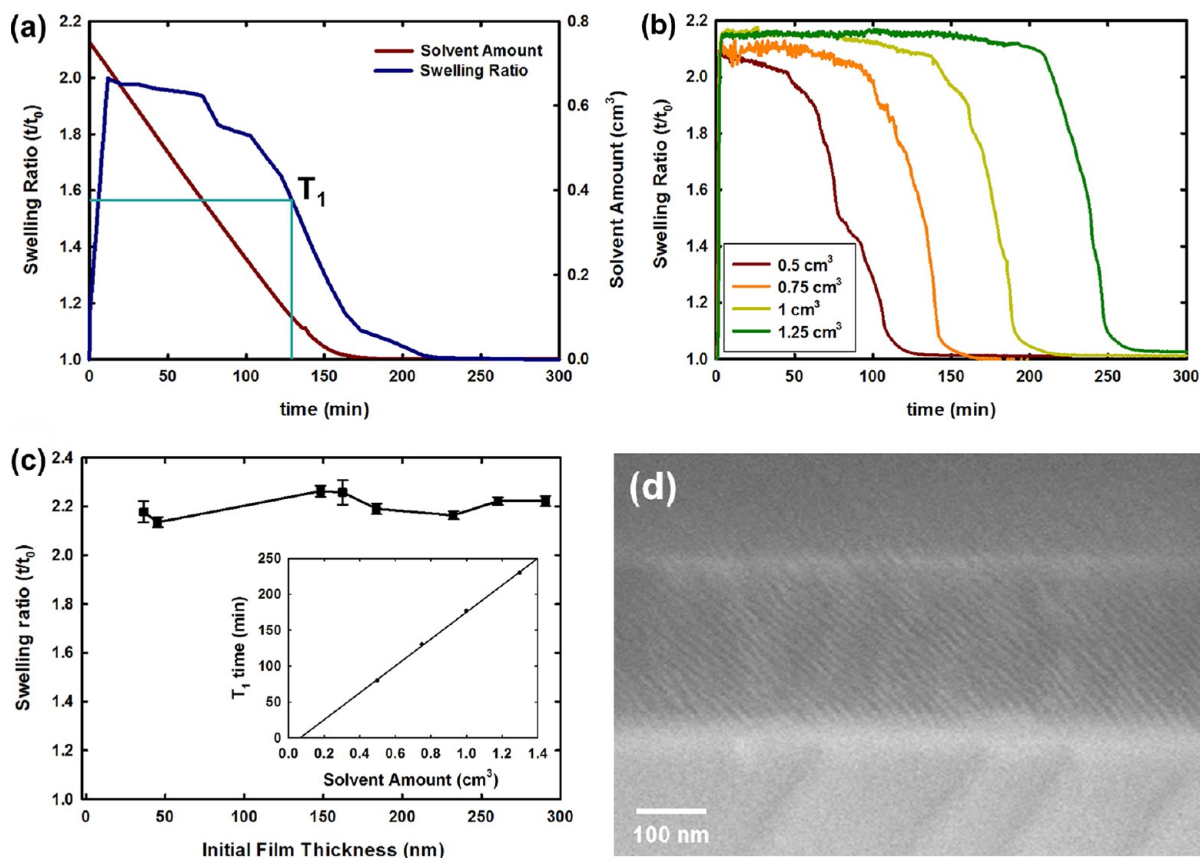

Figure 5. (a) Change in mass of solvent with time and swelling ratio of 380 nm thick SD45 annealed in 0.75 cm^3 chloroform. T_1 is the time at which the swelling ratio is 1.55, half of the maximum swelling ratio observed. (b) In situ swelling ratio of SD45 thin films vs time, corresponding to different initial solvent amounts. (c) Swelling ratio of SD45 film vs initial film thickness after 15 min of solvent annealing with 1 cm^3 of chloroform. Inset: A plot of T_1 vs initial solvent volume determined from the data in (b). (d) SD16 film after rapid drying with a nitrogen gun showing tilted cylinders.

to air led to a mixture of orientations of cylinders. Quenching using nitrogen blowing, as in Figure 5d, usually formed a tilted orientation in the bulk of the films and in-plane orientation at the top surface. When the film was initially swelled in a saturated vapor in a closed chamber and then rapidly quenched by exposing it to air, in-plane cylinders were observed.

We suggest that, in these thick films, a gradient in solvent concentration develops as solvent escapes from the top surface of the film, so the "solidification" boundary between block copolymer chains that are still mobile and those that have low diffusivity moves from the film surface to the substrate interface as drying proceeds.[24] In situ GISAXS measurements of BCP films[25] showed that films that swelled by a factor greater than about 2 can be well ordered in the swelled state, so it is likely that cylinders or lamellae were already present in the swelled films. Films initially swelled by 2.1−2.2 are assumed to have poorly ordered cylinders or lamellae, and slow drying allowed them to reorient perpendicular to the substrate. However, rapid quenching preserved a more random orientation or caused tilting, possibly from off-normal drying caused by the nitrogen jet. Films annealed at a higher swelling ratio (2.3−2.4) and a longer anneal time, or those thermally annealed, had already formed in-plane cylinders throughout the film thickness during the anneal, and this orientation was preserved during deswelling or rapid cooling.

Any tendency for perpendicular orientation promoted by the solvent anneal process had to compete with in-plane orientations promoted by the preferential wetting of PDMS at the air interface and at a PDMS-brushed substrate when the brush was used. In highly swelled films, or those annealed for a long time, this in-plane orientation propagated from the surface to the interior of the films, forming in-plane cylinders throughout the film thickness, whereas in the slowly dried films, the parallel orientation was only present at the surface(s). A related result was obtained from solvent-annealed PS-*b*-PEO with organosilicate films[14] in which an initial perpendicular orientation evolved into an in-plane orientation at the film surface with extended annealing time in a non-neutral solvent.

This simple picture is complicated by changes that may occur in the swelling ratio with film thickness[26] and a lower equilibrium solvent concentration near the substrate in thick films due to greater constraint of the polymer chains,[27] but it indicates that the time dependence of the solvent vapor pressure is a key determinant of the microdomain orientation.

Long range order is necessary for device applications, for example, in semiconductor devices or patterned media. To template the perpendicular microdomains, the substrate was patterned with topographical features made using hydrogen silsesquioxane (HSQ) resist exposed using electron beam lithography. After development, the HSQ formed a silica-like material. The posts were 10 nm tall and had a period of 38 nm (Figure 5a) or 30 nm (Figure 5c), a diameter of ∼10 nm, and covered an area equal to 10 μm^2. The SD16 cylindrical PS-*b*-PDMS block copolymer was spin-cast on the posts and solvent annealed, and then most of the film thickness was removed by etching so that the alignment of the perpendicular cylinders

near the substrate surface could be seen. In the 38 nm post array, the spacing was commensurate with the BCP = 2 L_0, and it is clear in Figure 5b that the microdomains subdivided the spacing of the posts to form a ⟨20⟩ lattice analogous to the templating of spherical microdomains by a post lattice.[20] In Figure 5d, the post lattice is incommensurate with L_0 (L_{post}/L_0 = 1.67), and commensurability arguments would suggest a ⟨11⟩ lattice would form. Figure 6d shows instead some evidence for in-plane segments of cylinders forming in between the posts. The electron-beam-irradiated regions of the HSQ tended to promote an in-plane cylinder orientation even on a substrate where perpendicular cylinders formed at the film−substrate interface.

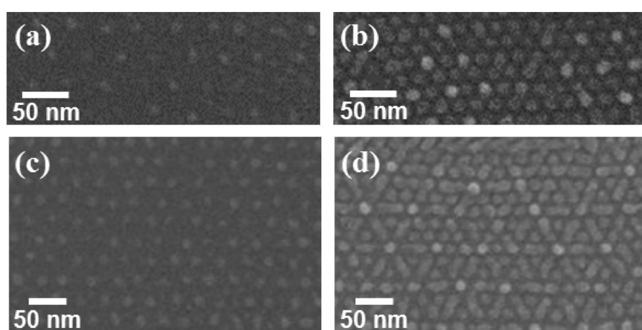

Figure 6. SEM images of (a) a 38 nm period of sparse hexagonal lattice of HSQ post templates and (b) a perpendicular oriented cylindrical morphology of solvent annealed 16 kg/mol PS-*b*-PDMS thin films on 38 nm period HSQ post arrays; (c) 30 nm period sparse hexagonal HSQ posts and (d) perpendicular oriented cylinder patterns from 16 kg/mol PS-*b*-PDMS on 30 nm period post arrays.

The proposed model for the slowly drying film would suggest that substrate patterning should be ineffective at templating the block copolymer because the film dries at the air interface first. However, it is likely that the substrate patterns influence the locations and orientations of the microdomains near the substrate leading to local registration of the microdomains. A more detailed cross-sectional study of the film would clarify the thickness of the film that is affected by the substrate pattern.

In summary, we demonstrated how perpendicularly oriented microdomains could be achieved in PS-*b*-PDMS block copolymers of different molecular weights and morphologies using a slowly drying vapor solvent annealing process. High-aspect-ratio nanostructures were obtained using a high power CF_4/O_2 RIE to remove the top layers of in-plane microdomains. The microdomains were templated locally by topographical features on the substrate. Using this approach, sub-10 nm diameter, high-aspect-ratio patterns from high χ PS-*b*-PDMS can be produced that may be useful in advanced nanolithography applications.

■ EXPERIMENTAL METHODS

Self-assembly of PS-*b*-PDMS films: PS-*b*-PDMS diblock copolymers with molecular weights of cylindrical 45.5 kg mol^{-1} (polydispersity index (PDI) ~ 1.15, f_{PS} ~ 0.68), 16 kg mol^{-1} (PDI ~ 1.08, f_{PS} ~ 0.69), and lamellar 43 kg mol^{-1} (PDI ~ 1.08, f_{PS} ~ 0.50) were purchased from Polymer Source, Inc. Supplier-provided size exclusion chromatography data indicated a single peak for the SD16, but a shoulder in the SD45 peak indicates the possible presence of homopolymer.

A total of 3−5 wt % of the PS-*b*-PDMS solution in cyclohexane was spin-coated on as-received Si substrates with thickness from 150 to 300 nm. Solvent annealing was carried out using acetone or chloroform in a 9.3 mL glass Petri disk with a cover until the solvent was fully evaporated, which took less than 4 h. The annealed BCP films were first treated with high power CF_4/O_2 RIE (30 s, 450 W) to etch the parallel oriented top layers (~120 nm) and then O_2 RIE (30 s, 90 W) to selectively remove the PS domains and make high-aspect-ratio nanopatterns.

Template preparation: The nanopost templates were fabricated using electron beam patterning of hydrogen silsesquioxane (HSQ), a negative-tone electron beam resist. HSQ films (FOx 1% solids from Dow Corning) were spin-coated on silicon substrates. Hexagonally arranged single-pixel dots were exposed in a Raith 150 electron-beam lithography tool at 30 kV acceleration voltage. The samples were developed in 0.25 M NaOH/0.7 M NaCl in distilled water to remove unexposed resist and to reveal the topographical nanostructures.

Characterization: To observe the morphology of the films at the film-substrate interface, a Si wafer with 50 nm thick SiO_2 layer was used as the substrate. The films were partially immersed in 5 wt % HF aqueous solution to dissolve the SiO_2 sacrificial layer and the released polymer film was flipped over to expose the bottom interface of the film. The morphology of the block copolymer patterns was observed by field emission-scanning electron microscope (FE-SEM, Zeiss/Leo Gemini 982) operated at 5 kV. The samples for FE-SEM were coated with a thin Au−Pd alloy film to avoid charging effects.

■ AUTHOR INFORMATION

Corresponding Author

*E-mail: caross@mit.edu.

Notes

The authors declare no competing financial interest.

■ ACKNOWLEDGMENTS

We gratefully acknowledge financial support from the Semiconductor Research Corporation and the FENA Center. Substrates were patterned using the Scanning-Electron-Beam Lithography Facility in the Research Laboratory of Electronics at MIT.

■ REFERENCES

(1) ITRS, International Technology Roadmap for Semiconductors, 2011 ed.; http://www.itrs.net/Links/2011ITRS/2011Chapters/2011ERM.pdf.

(2) Bang, J.; Jeong, U.; Ryu, D. Y.; Russell, T. P.; Hawker, C. J. *Adv. Mater.* **2009**, *21*, 4769−4792.

(3) Park, M.; Harrison, C.; Chaikin, P. M.; Register, R. A.; Adamson, D. H. *Science* **1997**, *276*, 1401−1404.

(4) Cheng, J. Y.; Ross, C. A.; Smith, H. I.; Thomas, E. L. *Adv. Mater.* **2006**, *18*, 2505−2521.

(5) Lazzari, M.; López-Quintela, M. A. *Adv. Mater.* **2003**, *15*, 1583−1594.

(6) Cheng, J. Y.; Ross, C. A.; Thomas, E. L.; Smith, H. I.; Vancso, G. J. *Adv. Mater.* **2003**, *15*, 1599−1602.

(7) Thurn-Albrecht, T.; Schotter, J.; Kästle, G. A.; Emley, N.; Shibauchi, T.; Krusin-Elbaum, L.; Guarini, K.; Black, C. T.; Tuominen, M. T.; Russell, T. P.; Kastle, G. A. *Science* **2000**, *290*, 2126−2129.

(8) Huang, E.; Rockford, L.; Russell, T. P.; Hawker, C. J. *Nature* **1998**, *395*, 757−758.

(9) Sivaniah, E.; Hayashi, Y.; Matsubara, S.; Kiyono, S.; Hashimoto, T.; Fukunaga, K.; Kramer, E. J.; Mates, T. *Macromolecules* **2005**, *38*, 1837−1849.

(10) Son, J. G.; Bulliard, X.; Kang, H.; Nealey, P. F.; Char, K. *Adv. Mater.* **2008**, *20*, 3643−3648.

(11) Jung, Y. S.; Ross, C. A. *Nano Lett.* **2007**, *7*, 2046−2050.

(12) Kim, S. H.; Misner, M. J.; Xu, T.; Kimura, M.; Russell, T. P. *Adv. Mater.* **2004**, *16*, 226−231.

(13) Bang, J.; Kim, S. H.; Drockenmuller, E.; Misner, M. J.; Russell, T. P.; Hawker, C. J. *J. Am. Chem. Soc.* **2006**, *128*, 7622−7629.
(14) Freer, E. M.; Krupp, L. E.; Hinsberg, W. D.; Rice, P. M.; Hedrick, J. L.; Cha, J. N.; Miller, R. D.; Kim, H.-C. *Nano Lett.* **2005**, *5*, 2014−2018.
(15) Nose, T. *Polymer* **1995**, *36*, 2243−2248.
(16) Jung, Y. S.; Chang, J. B.; Verploegen, E.; Berggren, K. K.; Ross, C. A. *Nano Lett.* **2010**, *10*, 1000−1005.
(17) Jung, Y. S.; Ross, C. A. *Adv. Mater.* **2009**, *21*, 2540−2545.
(18) Yang, J. K. W.; Jung, Y. S.; Chang, J.-B.; Mickiewicz, R. A.; Alexander-Katz, A.; Ross, C. A.; Berggren, K. K. *Nat. Nanotechnol.* **2010**, *5*, 256−260.
(19) Jung, Y. S.; Ross, C. A. *Small* **2009**, *5*, 1654−1659.
(20) Bita, I.; Yang, J. K. W.; Jung, Y. S.; Ross, C. A.; Thomas, E. L.; Berggren, K. K. *Science* **2008**, *321*, 939−943.
(21) Son, J. G.; Chang, J.-B.; Berggren, K. K.; Ross, C. A. *Nano Lett.* **2011**, *11*, 5079−5084.
(22) Son, J. G.; Hannon, A. F.; Gotrik, K. W.; Alexander-Katz, A.; Ross, C. A. *Adv. Mater.* **2011**, *23*, 634−639.
(23) Wu, S. In *Polymer Handbook*; Brandrup, J., Immergut, E. H., Grulke, E. A., Abe, A., Bloch, D. R., Eds.; John Wiley & Sons: New York, 2005; pp 521−541.
(24) Albert, J. N. L.; Young, W.-S.; Lewis, R. L.; Bogart, T. D.; Smith, J. R.; Epps, T. H. *ACS Nano* **2012**, *6*, 459−466.
(25) Paik, M. Y.; Bosworth, J. K.; Smilges, D.-M.; Schwartz, E. L.; Andre, X.; Ober, C. K. *Macromolecules* **2010**, *43*, 4253−4260.
(26) Zettl, U.; Knoll, A.; Tsarkova, L. *Langmuir* **2010**, *26*, 6610−6617.
(27) Mukherjee, M.; Singh, A.; Daillant, J.; Menelle, A.; Cousin, F. *Macromolecules* **2007**, *40*, 1073−1080.